JACS
JOURNAL OF THE AMERICAN CHEMICAL SOCIETY
Article
Cite This: J. Am. Chem. Soc. 2019, 141, 1614−1627
pubs.acs.org/JACS

Mechanism and Kinetics of Propane Dehydrogenation and Cracking over Ga/H-MFI Prepared via Vapor-Phase Exchange of H-MFI with $GaCl_3$

Neelay M. Phadke,[†,⊥] Erum Mansoor,[†,⊥] Matthieu Bondil,[‡] Martin Head-Gordon,[§] and Alexis T. Bell*[,†]

[†]Department of Chemical and Biomolecular Engineering, University of California, Berkeley, California 94720, United States
[‡]Ecole Polytechnique Federale de Lausanne, Lausanne, Switzerland CH-1015
[§]Department of Chemistry, University of California, Berkeley, California 94720, United States

Supporting Information

ABSTRACT: In this study, the mechanism and kinetics of C_3H_8 dehydrogenation and cracking are examined over Ga/H-MFI catalysts prepared via vapor-phase exchange of H-MFI with $GaCl_3$. The present study demonstrates that $[GaH]^{2+}$ cations are the active centers for C_3H_8 dehydrogenation and cracking, independent of the Ga/Al ratio. For identical reaction conditions, $[GaH]^{2+}$ cations in Ga/H-MFI exhibit a turnover frequency for C_3H_8 dehydrogenation that is 2 orders of magnitude higher and for C_3H_8 cracking, that is 1 order of magnitude higher than the corresponding turnover frequencies over H-MFI. C_3H_8 dehydrogenation and cracking exhibit first-order kinetics with respect to C_3H_8 over H-MFI, but both reactions exhibit first-order kinetics over Ga/H-MFI only at very low C_3H_8 partial pressures and zero-order kinetics at higher C_3H_8 partial pressures. H_2 inhibits both reactions over Ga/H-MFI. It is also found that the ratio of the rate of dehydrogenation to the rate of cracking over Ga/H-MFI is independent of C_3H_8 and H_2 partial pressures but weakly dependent on temperature. Measured activation enthalpies together with theoretical analysis are consistent with a mechanism in which both the dehydrogenation and cracking of C_3H_8 proceed over Ga/H-MFI via reversible, heterolytic dissociation of C_3H_8 at $[GaH]^{2+}$ sites to form $[C_3H_7\text{-}GaH]^{+}\text{-}H^{+}$ cation pairs. The rate-determining step for dehydrogenation is the β-hydride elimination of C_3H_6 and H_2 from the C_3H_7 fragment. The rate-determining step for cracking is C−C bond attack of the same propyl fragment by the proximal Brønsted acid O−H group. H_2 inhibits both dehydrogenation and cracking over Ga/H-MFI via reaction with $[GaH]^{2+}$ cations to form $[GaH_2]^{+}\text{-}H^{+}$ cation pairs.

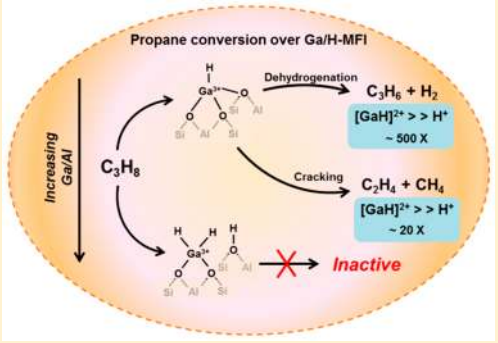

1. INTRODUCTION

The increasing availability of large shale gas reserves in the U.S. and across the world has stimulated interest in finding routes for the catalytic conversion of the condensable components of shale gas, principally ethane and propane, to alkenes and aromatics via dehydrogenation and dehydrocyclization, respectively.[1−5] Commercially implemented processes[6] include the Oleflex and Catofin processes for dehydrogenation, which utilize alumina-supported catalysts and also the Cyclar and Aroforming processes, which use metal-modified zeolite catalysts for dehydroaromatization. Gallium-exchanged H-MFI zeolite (Ga/H-MFI) has been shown to be particularly effective for catalyzing alkane dehydroaromatization.[5,7−11] For example, reactions of C_3H_8 over Ga/H-MFI result in higher selectivities to alkenes and aromatics than those observed over unmodified H-MFI.[10,12] This has led to a renewed interest in studying the structure and catalytic role of Ga species in Ga/H-MFI, as active sites for light alkane conversion.[13−22]

The chemical structure and catalytic function of Ga cations in Ga/H-MFI have been examined both experimentally and theoretically.[23] These studies suggest that in the oxidized or reduced state, the following types of species may exist in Ga/H-MFI: $[GaO]^{+}$, $[Ga_2O_2]^{+}$, $[Ga(OH)]^{2+}$, $[Ga(OH)_2]^{+}$, $[GaH_2]^{+}$, $[GaH]^{2+}$, Ga^{+}, and GaO_x clusters.[9,24−32] It should be noted that with the exception of Ga^{+}, the oxidation state of Ga in all of the other proposed structures is +3. Earlier studies of light alkane dehydrogenation over Ga/H-MFI have reported that oxygen-ligated species, such as monomeric $[GaO]^{+}$ or dimeric $[Ga_2O_2]^{2+}$ cations, are more active than reduced Ga^{+} cations.[26,29−31] However, contemporaneous studies as well as more recent ones have suggested that Ga^{+} cations are the active centers for alkane dehydrogenation.[9,10,15,28,29,33,34] A variant of this idea has also been recently proposed, namely, that Ga^{+} cations in proximity to Brønsted acid O−H groups catalyze C_3H_8 dehydrogenation via oxidative addition of H^{+} to Ga^{+} to form a highly Lewis acidic $[GaH]^{2+}$ species in which the Ga^{3+} center has an oxidation state of +3.[22] The role of $[GaH]^{2+}$

Received: October 23, 2018
Published: December 26, 2018

DOI: 10.1021/jacs.8b11443
J. Am. Chem. Soc. 2019, 141, 1614−1627

cations as the active center for alkane dehydrogenation has also been supported by theoretical studies. These studies show that divalent $[GaH]^{2+}$ cations, located at proximate cation-exchange sites in Ga/H-MFI, are more active for light alkane dehydrogenation than monovalent $[GaH_2]^+$ cations or Ga^+ cations.[22,32,35,36]

While a number of authors have proposed that Ga^+ cations are active for the dehydrogenation of light alkanes,[9,10,15,28,29,33,34,37] the presence of Ga^+ cations in H_2-reduced Ga/H-MFI has been disputed. Recent work by Getsoian et al. has called into question the interpretation of XANES evidence for Ga^+ cations.[18] These authors note that the decreases in the Ga K-edge XANES edge energy of Ga/H-MFI upon reduction, previously ascribed to formation of Ga^+,[9,10] can be ascribed, instead, to the formation of Ga-alkyl or GaH_x species, in which Ga has a formal oxidation state of +3.[18] Theoretical studies have also shown that the activation barrier for the formation of Ga^+ species in Ga/H-MFI is considerably higher than that for the formation of GaH_x species in which the Ga center has a formal oxidation state of +3.[36,38]

A further issue complicating the identification of the catalytically active species in Ga/H-MFI is the synthetic protocol typically employed for the preparation of Ga/H-MFI: incipient wetness impregnation of H-MFI with an aqueous solution of a Ga salt, most notably $Ga(NO_3)_3$.[39] Steric and electronic constraints associated with large aqueous Ga^{3+} complexes result in a slow diffusion of Ga into the MFI micropores, leading to low levels of ion exchange and the deposition of GaO_x agglomerates at the external surfaces of the zeolite crystal.[23,40] Upon contact with H_2 or alkane reactants at reaction temperatures (>700 K), ion exchange has been reported to occur via conversion of GaO_x into volatile Ga_2O monomers.[9] However, the resulting materials have been reported to still contain detectable concentrations of GaO_x.[40] The presence of neutral GaO_x together with ion-exchanged Ga^{3+} cations in Ga/H-MFI prepared via the conventional protocol has precluded accurate determination of the active Ga structures and their catalytic role in light alkane dehydrogenation and dehydroaromatization.

We report here a detailed study of the mechanism and kinetics of C_3H_8 dehydrogenation and cracking over Ga/H-MFI with Ga/Al ratios ranging from 0.05 to 0.5. These catalysts were prepared by reaction of the Brønsted acid O−H groups in H-MFI with $GaCl_3$ vapor under anhydrous conditions at elevated temperature, followed by stoichiometric removal of Ga-bound Cl by H_2 reduction, resulting in the formation of GaH_x (x = 1, 2) structures. Detailed characterization of these samples shows that for Ga/Al ratios below 0.3, and upon reduction under anhydrous conditions, all of the Ga is present as isolated $[GaH]^{2+}$ cations or as $[GaH_2]^+$-H^+ cation pairs; neutral GaO_x agglomerates are undetectable in these samples.[41] Both types of cationic species are associated with proximate cation-exchange sites associated with NNN (next nearest neighboring, i.e., separated by a −O−Si−O linkage) or NNNN (next, next nearest neighboring, i.e., separated by a −O−Si−O−Si−O linkage) pairs of framework Al atoms. Our investigations show that C_3H_8 dehydrogenation over these samples of Ga/H-MFI occurs primarily over $[GaH]^{2+}$ cations, independent of the Ga/Al ratio, at a rate (per Al_{tot} atom) that is 2 orders of magnitude higher than that occurring over isolated Brønsted acid O−H groups located in H-MFI, under identical reaction conditions. The rate of C_3H_8 cracking to CH_4 and C_2H_4 over Ga/H-MFI is an order of magnitude higher than that over H-MFI and also occurs over $[GaH]^{2+}$ sites. While both cracking and dehydrogenation rates exhibit first-order dependences on C_3H_8 partial pressure over H-MFI, the rates of both reactions exhibit a Langmuir−Hinshelwood dependence on C_3H_8 partial pressure over Ga/H-MFI and are inhibited by H_2. Over H-MFI, both the dehydrogenation and cracking of C_3H_8 occur over Brønsted acid O−H groups. In the case of Ga/H-MFI, examination of alternative reaction pathways via experiment and theory suggests that both reactions occur preferentially on $[GaH]^{2+}$ sites via mechanisms involving C_3H_8-derived $[C_3H_7\text{-}GaH]^+$ intermediates. Inhibition of both reactions by H_2 is proposed to occur via the formation of $[GaH_2]^+$-H^+ cation pairs.

2. EXPERIMENTAL AND THEORETICAL METHODS

2.1. Preparation of H-MFI and Ga/H-MFI. NH_4-MFI (Zeolyst, CBV 3024E) was converted to the H-form by heating it at 2 K min^{-1} to 773 K in dry synthetic air (Praxair, ultrazero, 100 cm^3 min^{-1}) and then holding it at this temperature for 4 h. The Si/Al_{tot} ratio of this sample is 16.5 ± 1.0, as determined by ICP-OES (Galbraith Laboratories, Knoxville, TN, USA). Ga/H-MFI samples with varying Ga/Al ratios (0.05−0.5) were prepared via anhydrous exchange of dehydrated H-MFI with $GaCl_3$ vapor, using a protocol developed by our group. A detailed discussion of the preparation and characterization of these samples is given in ref 41.

2.2. Reaction Rate Measurements. Reaction rates for C_3H_8 conversion over H-MFI and Ga/H-MFI were measured using a tubular quartz plug flow reactor. Catalyst samples (∼5−12 mg) were placed over a quartz wool plug, fitted inside the reactor (30.5 cm in length and 0.64 cm in outer diameter). Catalyst charges less than 8 mg were diluted with SiO_2 (Silia Flash 150A). The reactor was heated by means of a ceramic cylindrical furnace. The temperature of the catalyst bed was measured by a K-type thermocouple (Omega) connected to a temperature controller (Omega), to maintain the catalyst temperature. Gases were metered into the reactor by means of mass flow controllers (MFCs) (Porter), which were calibrated using a bubble flow meter. Prior to making rate measurements, samples were heated at 2 K min^{-1} from ambient temperatures to 773 K under flowing dry synthetic air (Praxair, ultrazero, 100 cm^3 min^{-1}) and held at this temperature for 1 h. This oxidative pretreatment was used for H-MFI and Ga/H-MFI. Reductive pretreatment of Ga/H-MFI was carried out by purging the system with He following the oxidative treatment at 773 K and then switching the reactor feed to a gas mixture of 2.5% H_2 diluted in He (Praxair, CSG, 100 cm^3 min^{-1}). Samples were held at this temperature under H_2 for 1 h.

Following either oxidative or reductive pretreatments, samples were exposed to flowing mixtures of C_3H_8/He prepared by diluting a 20% C_3H_8/He stream (Praxair, CSG) with He (Praxair, UHP) in order to generate C_3H_8 partial pressures ranging from 0.25 to 11 kPa. Experiments involving co-fed H_2 were conducted by adding H_2 to the feed flow. For this purpose, a 2.5% H_2/He stream (Praxair, CSG) was mixed with the C_3H_8/He stream in order to obtain H_2 partial pressures ranging from 0.25 to 1.5 kPa. The total pressure of the system was maintained at 101.32 kPa. He, H_2, and dry synthetic air were further purified by passing these gases through purifiers (VICI) in order to remove trace amounts of H_2O or hydrocarbons. Gas flow rates were varied (100−350 cm^3 min^{-1}) in order to measure catalyst activity at different space times (defined as mol Al_{tot}·s/mol C_3H_8) for a given C_3H_8/H_2/He feed composition. A heated line connected to the outlet of the reactor was used to transfer reactants and reaction products to a gas chromatograph (GC) (Agilent 7890A). The reactor effluent present in a sample loop was injected periodically into the GC. Reactants and products were separated by a capillary column (Agilent 1909IP-Q02, 25 m × 350 μm × 10 μm) and were detected by means of a flame ionization detector (FID). FID response factors for hydrocarbons species were obtained by diluting a precalibrated gas mixture containing CH_4, C_2H_6, C_2H_4, C_3H_8, C_3H_6, C_4H_{10}, and C_4H_8

DOI: 10.1021/jacs.8b11443
J. Am. Chem. Soc. 2019, 141, 1614−1627

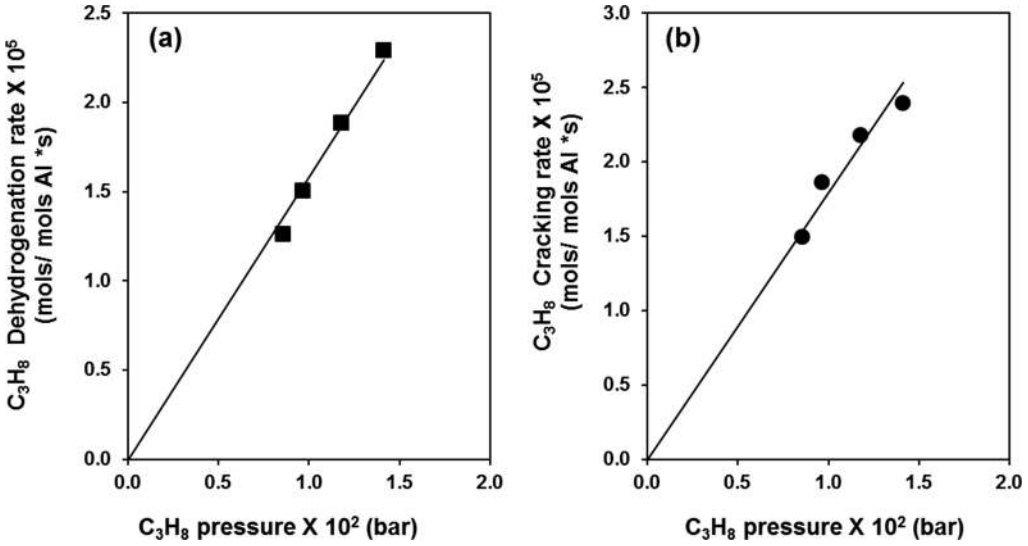

Figure 1. (a) Dependence of C_3H_8 dehydrogenation rates (per Al_{tot} atom) on C_3H_8 partial pressure measured over H-MFI at 733 K. (b) Dependence of C_3H_8 cracking rates (per Al_{tot} atom) on C_3H_8 partial pressure measured over H-MFI at 733 K. Solid lines indicate regressed first-order slopes.

with He to attain different concentrations of the component hydrocarbons. The response factors for C_6H_6 and C_7H_8 were determined by directly injecting known amounts of liquid C_6H_6 and C_7H_8 into the GC injector.

The conversion of C_3H_8 over H-MFI and Ga/H-MFI was measured at differential conversions (<9% C_3H_8 conversion) at temperatures between 718 and 753 K. Plots of conversion vs space time were linear for each feed composition combination and extrapolated to zero conversion at zero space time, consistent with reactor operation under a differential conversion regime. Selectivities were defined on both a C basis and C_3H_8 basis. C_3H_8 dehydrogenation rates were determined from C_3H_6 concentrations, while C_3H_8 cracking rates were determined from the concentrations of either CH_4 or C_2H_4 cracking products. When product selectivities were extrapolated to zero space time, cracking rates derived from CH_4 concentrations were similar to those determined from C_2H_4 concentrations. The C_3H_8 partial pressures (0.25−11 kPa) and H_2 partial pressures (0.25−1.5 kPa) were varied in a nonsystematic fashion in order to examine the effects of reactant and product pressures on measured rates. For each combination of C_3H_8/H_2 partial pressures, rates were measured at four different space times. By this means, rates could be extrapolated linearly to 0 space time. Moreover, after measurements had been made at each C_3H_8/H_2 pressure combination, rates were measured at 0.9 kPa C_3H_8/He at a space time of 9 mol Al·s/mol C_3H_8 in order to assess and correct for catalyst deactivation. Catalyst deactivation did not exceed 5% in typical experiments. Activation enthalpies and entropies were extracted by relations (eqs S24−S26) derived from transition state theory.[42] For the application of these equations, rate coefficients (per Al_{tot} atom) were normalized by the fraction of $[GaH]^{2+}$ cations per Al_{tot} atom determined via NH_3-TPD measurements (details described in the SI).[41]

2.3. Theoretical Methods. The hybrid quantum mechanics/molecular mechanics (QM/MM)[43,44] approach used in this work takes into account the impact of long-range dispersive interactions and the polarization of the active site by the electrostatic field associated with the zeolite lattice, both of which are critical to capturing reaction energetics accurately.[45] A T437 atom cluster was used to represent the zeolite framework surrounding the active site. The QM region consists of either a T5 or a T9 cluster representing the part of the zeolite associated with the extra-framework cation (H^+ or $[Ga(H)_n]^{(3-n)+}$) and any adsorbed species. The MM region was modeled with an improved parametrization;[46] framework Si and O atoms were fixed at their crystallographic positions. The framework Al atom associated with extra-framework Ga cationic species was taken to be at the T12 site. This T site is located in the channel intersections of MFI.[47] The activities of both Brønsted acid O−H groups and Lewis acidic $[GaH]^{2+}$ cations were investigated. As shown previously, only a small difference (2.6 kcal/mol) was found in the calculated barriers for C_2H_4 methylation over H-MFI calculated for both T5 and T20 clusters,[48] which suggests that our QM/MM approach is not influenced significantly by the size of the QM region used. An illustration of the model used for the $[GaH]^{2+}$ cation in this study is shown in Figure S.5 and is discussed in more detail in earlier work.[36]

Stationary and saddle point searches were conducted at the ωB97X-D/6-31G** level of theory using the default optimization procedure available in QChem.[49] The reported activation energies were computed using the ωB97X-D functional[50] with the triple-ζ, split-valence Pople basis set, with diffuse and polarization functions 6-311++G(3df,3pd). While recent developments in density functional theory (DFT) have led to functionals with statistically improved accuracy[51,52] relative to ωB97X-D, we note that the QM/MM parameters were developed specifically for that functional. Enthalpy and entropy calculations were performed using the quasi rigid rotor harmonic oscillator (RRHO) approximation. We have used this approach successfully in previous studies to obtain activation enthalpies and entropies for n-C_4H_{10} reactions in H-MFI, yielding good agreement with experimental results.[53] For each mechanism examined, we determined the value of $\Delta G^{\ddagger}$ from the respective free energy surface using the energetic span model proposed by Kozuch and Shaik.[54−57]

3. RESULTS AND DISCUSSION

3.1. C_3H_8 Conversion over H-MFI via Monomolecular Dehydrogenation and Cracking. For times-on-stream < 100 min, the rate of C_3H_8 dehydrogenation over H-MFI decreased monotonically, before approaching a steady state (see Figure S.1). However, the rate of C_3H_8 cracking did not change appreciably with time-on-stream. These trends are similar to those reported for n-C_4H_{10} dehydrogenation and cracking over H-MFI.[58] The authors of that study proposed that the high initial rate of n-C_4H_{10} dehydrogenation is attributable to Lewis acidic, extra-framework Al (EFAl) sites that deactivate during the first 100 min of reaction. All steady-state rates were therefore measured over H-MFI, after the deactivation period (~100 min).

DOI: 10.1021/jacs.8b11443
J. Am. Chem. Soc. 2019, 141, 1614−1627

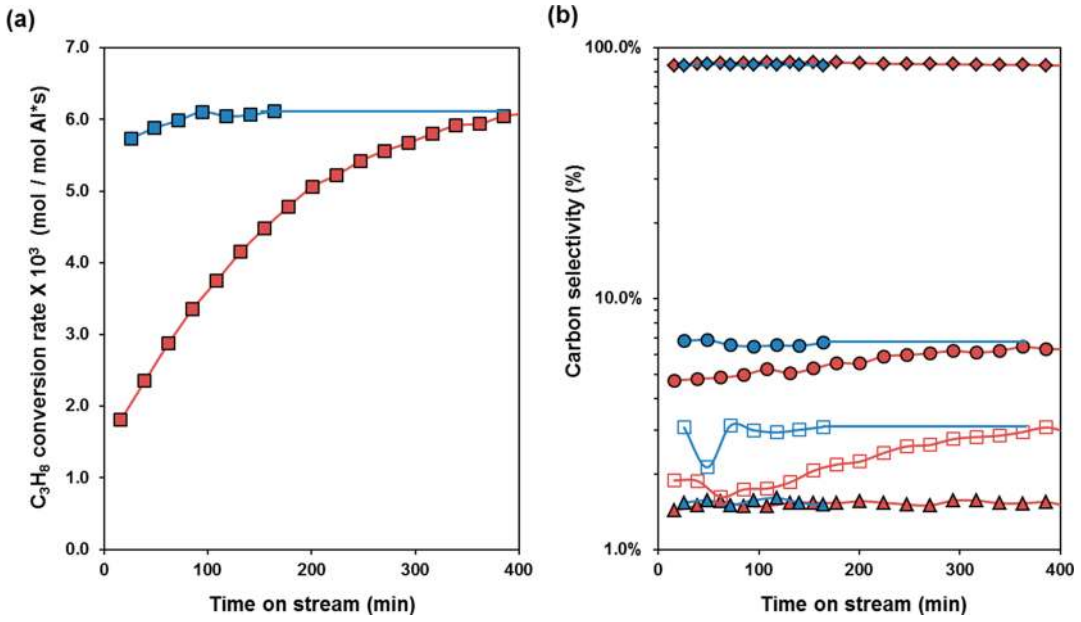

Figure 2. (a) C_3H_8 consumption rates (per Al_{tot} atom) and (b) percent carbon selectivities for Ga/H-MFI (Ga/Al = 0.2) measured at 733 K with 0.9 kPa C_3H_8/He and τ = 9 (mol Al·s/mol C_3H_8) space time. Blue data points indicate Ga/H-MFI pretreated in 2.5% H_2/He at 773 K for 1 h prior to reaction, while red data points indicate Ga/H-MFI pretreated in synthetic dry air at 773 K for 1 h prior to reaction. In Figure 2b, diamonds indicate C_3H_6, circles indicate C_2H_4, open squares indicate aromatics, and triangles indicate CH_4 selectivities.

The steady-state product molar ratios of H_2/C_3H_6 and C_2H_4/CH_4 during C_3H_8 conversion over H-MFI were close to unity, consistent with previous studies of C_3H_8 dehydrogenation and cracking over H-MFI.[58−60] As seen in Figure 1a and b, the rates of both dehydrogenation and cracking are first-order in C_3H_8 partial pressure, also in agreement with previous reports for monomolecular dehydrogenation and cracking catalyzed by Brønsted acid O−H groups at low alkane partial pressures.[61,62]

Apparent first-order rate coefficients were measured at different temperatures (see Figure S.2.), and these data were used to determine apparent activation enthalpies (ΔH_{app}) for C_3H_8 dehydrogenation and cracking. The experimentally measured apparent activation enthalpies for C_3H_8 dehydrogenation and cracking were found to be 40.6 ± 2.9 and 34.6 ± 3.8 kcal/mol, respectively (reported uncertainties reflect 95% confidence intervals). Both estimates are consistent with previous reported estimates of activation energies for C_3H_8 monomolecular dehydrogenation (22.7−47.8 kcal/mol) and monomolecular cracking (35.1−37.7 kcal/mol) over H-MFI.[59,60,63,64] We also obtained theoretical estimates of apparent activation enthalpies for these reactions occurring over isolated Brønsted acid O−H groups in H-MFI via QM/MM calculations. Apparent activation enthalpies estimated in this manner are 47.5 kcal/mol for methyl C-H activated C_3H_8 dehydrogenation, 35.3 kcal/mol for methylene C-H activated C_3H_8 dehydrogenation, and 33.3 kcal/mol for C_3H_8 cracking. The activation enthalpy for methylene-C_3H_8 dehydrogenation is expected to be significantly lower than that for methyl C_3H_8-dehydrogenation, due to the higher stability of the secondary carbenium ion formed in the late dehydrogenation transition state of the former pathway relative to the primary carbenium formed in the late dehydrogenation transition state of the latter pathway. Consistent with this interpretation, our experimental measurements are in good agreement with theoretical predictions for methylene dehydrogenation and cracking. The transition state structures and free energy surfaces for these mechanisms are presented in Figures S.13 and S.14 of the SI.

3.2. C_3H_8 Conversion over Oxidized and H_2-Reduced Ga/H-MFI. Figure 2a shows the rates of C_3H_8 consumption at 733 K over Ga/H-MFI (Ga/Al = 0.2) under differential reaction conditions (C_3H_8 conversion <9%). Following oxidative pretreatment of Ga/H-MFI (at 773 K in flowing dry air for 1 h), the rate of C_3H_8 consumption increases monotonically with time-on-stream for ∼300 min before approaching a steady state (red curve, Figure 2a). This slow induction period suggests that Ga species undergo structural transformation before reaching their steady-state structure. Also shown in Figure 2a is the rate of C_3H_8 consumption as a function of time-on-stream for Ga/H-MFI (Ga/Al = 0.2) reduced in 2.5% H_2/He for 1 h at 773 K prior to measurements of the reaction rate (blue curve, Figure 2a). In this case, no induction period is observed and the steady-state rate of C_3H_8 consumption is nearly identical to that measured over the oxidized sample.

Product selectivities (expressed as the fraction of converted carbon in each product) are shown as a function of time-on-stream in Figure 2b, for oxidized and H_2-reduced Ga/H-MFI. Throughout the duration of the experiment, the dominant product is C_3H_6, produced via C_3H_8 dehydrogenation. The selectivity to C_3H_6 does not change with time-on-stream or catalyst pretreatment. The same is true for the selectivity to CH_4. For the oxidized sample, the selectivities to C_2H_4 and aromatics increase slightly as a function of time-on-stream, but approach the same values as that observed for the reduced sample. While C_2H_4 is formed as a primary product via cracking of C_3H_8, space time studies (see Section S.3) indicate that C_2H_4 is also produced via secondary pathways at higher conversions. These experiments also show that aromatics are produced exclusively via secondary pathways, which become increasingly prevalent at higher conversion. Therefore, the

DOI: 10.1021/jacs.8b11443
J. Am. Chem. Soc. 2019, 141, 1614−1627

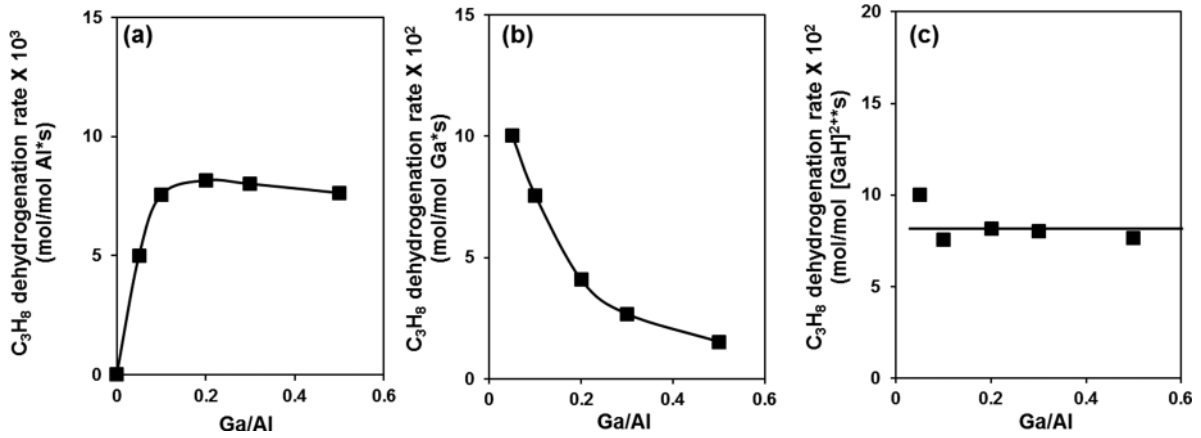

Figure 3. C_3H_8 dehydrogenation rates, measured at 0.9 kPa C_3H_8/He and 733 K as a function of Ga/Al ratio, with rates over Ga/H-MFI extrapolated to zero space time. (a) Rates normalized per Al_{tot} atom. (b) Rates normalized per Ga atom. (c) Rates normalized per $[GaH]^{2+}$ estimated via NH_3-TPD.[41] Solid lines are guides for the eye.

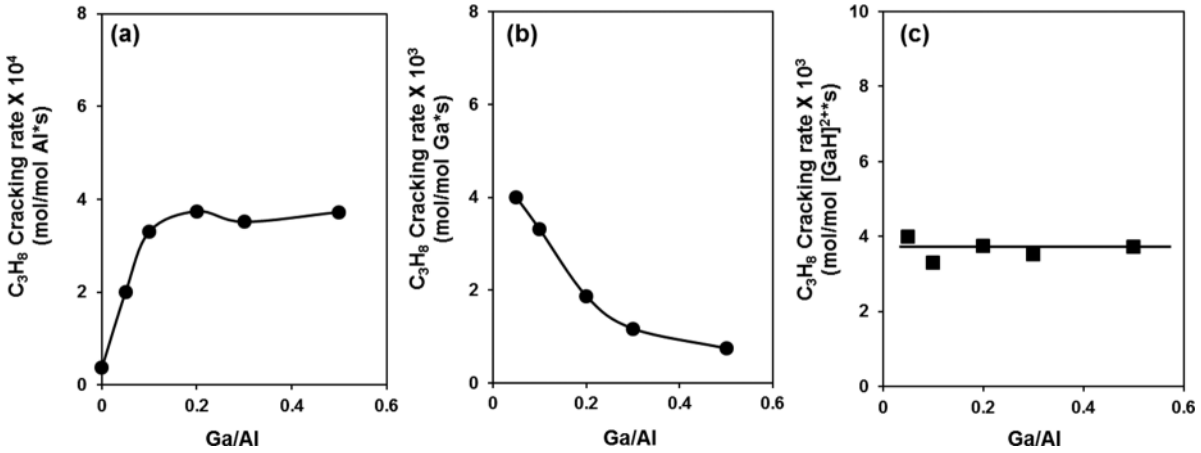

Figure 4. C_3H_8 cracking rates over H-MFI and Ga/H-MFI, measured at 0.9 kPa C_3H_8/He and 733 K. Rates over Ga/H-MFI were extrapolated to zero space time. (a) Rates normalized per Al_{tot} atom. (b) Rates normalized per Ga atom. (c) Rates normalized per $[GaH]^{2+}$ estimated via NH_3-TPD measurements. Dotted lines are guides for the eye.

concentrations of both C_2H_4 and aromatics are expected to increase as the rate of C_3H_8 consumption over oxidized Ga/H-MFI increases with time-on-stream. Thus, the product selectivity trends seen in Figure 2b suggest that similar active sites catalyze C_3H_8 dehydrogenation and cracking and that the concentration of these active sites increases with time-on-stream for oxidized Ga/H-MFI or upon prereduction of the catalyst in H_2.

The results presented in Figure 2, together with our earlier characterization work,[41] suggest that $[GaH]^{2+}$ cations and/or $[GaH_2]^+$-H^+ cation pairs formed upon H_2 reduction of Ga/H-MFI are the active species for C_3H_8 dehydrogenation and cracking. We propose that during the induction period observed over oxidized Ga/H-MFI, $[Ga(OH)]^{2+}$ cations and $[Ga(OH)_2]^+$-H^+ cation pairs undergo reduction to form $[GaH]^{2+}$ cations and $[GaH_2]^+$-H^+ cation pairs.

As shown in Section S.3, secondary reactions are prevalent even under conditions of differential conversion. We also show in Figure S.4 and Section 3.4 that the rates of dehydrogenation and cracking over Ga/H-MFI are inhibited by H_2. To eliminate the effects of product inhibition and secondary reactions, all of the steady-state measured reaction rates reported in the balance of this study were extrapolated to zero space time (see Figure S.4).

3.3. Effects of Ga Content on the Rates of C_3H_8 Dehydrogenation and Cracking over Ga/H-MFI. Figures 3a–c and 4a–c show C_3H_8 dehydrogenation and cracking rates, measured at 733 K and 0.9 kPa C_3H_8/He over H-MFI and Ga/H-MFI, as functions of the Ga/Al ratio. As observed in Figure 3a, the rate of C_3H_8 dehydrogenation (normalized per Al_{tot} atom) increases with Ga content up to a Ga/Al ratio of 0.1 but then reaches a plateau for higher values of Ga/Al ratio. At this plateau, the rate of C_3H_8 dehydrogenation is ~500 times higher than the corresponding rate over H-MFI, suggesting that the reactivity contribution of residual Brønsted acid O–H acid groups in Ga/H-MFI is negligible.

The rate of C_3H_8 dehydrogenation over Ga/H-MFI can also be normalized per Ga atom by dividing the rate per Al_{tot} by the Ga/Al_{tot} ratio. The rate of C_3H_8 dehydrogenation normalized this way, shown in Figure 3b, decreases monotonically as the Ga/Al ratio increases from 0.05 to 0.5, suggesting that the most active Ga species exist at the lowest Ga/Al ratios. As discussed earlier, our characterization of H_2-reduced Ga/H-MFI samples used in the present study shows that for Ga/Al ≤ 0.3 the dominant Ga species present are $[GaH]^{2+}$ cations and $[GaH_2]^+$-H^+ cation pairs and that 100% of the Ga is present as $[GaH]^{2+}$ cations for Ga/Al = 0.1.[41] Moreover, the theoretical calculations supporting this work show that the formation of

DOI: 10.1021/jacs.8b11443
J. Am. Chem. Soc. 2019, 141, 1614–1627

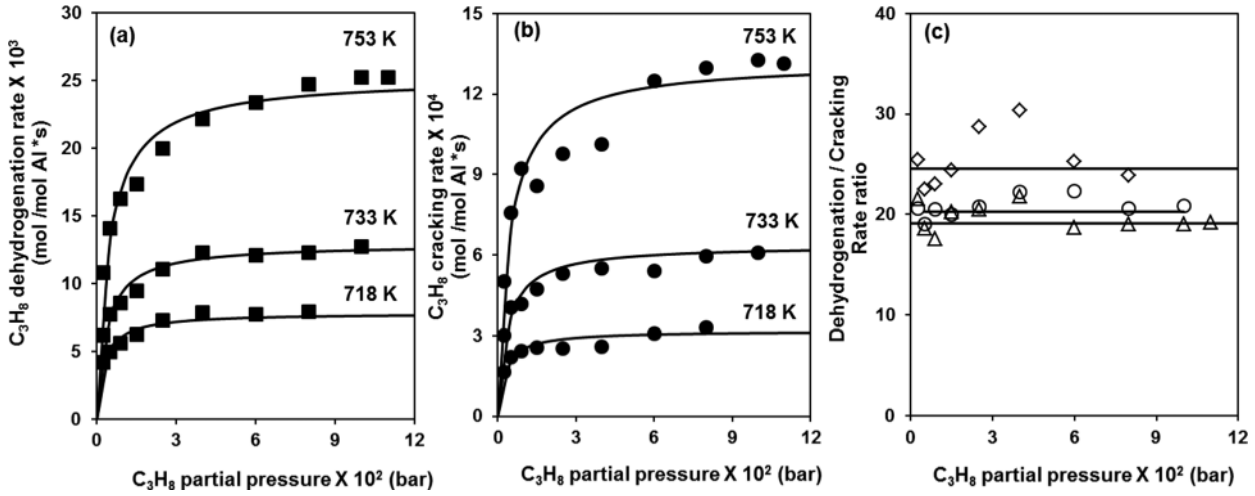

Figure 5. (a) Dependence of the rates of C_3H_8 dehydrogenation and (b) C_3H_8 cracking and (c) the ratio of the rates of dehydrogenation to cracking over Ga/H-MFI (Ga/Al = 0.2) measured at 718, 733, and 753 K, on the C_3H_8 partial pressure. In Figure 5c, triangles, circles, and diamonds indicate the ratios of rates at 718, 733, and 753 K, respectively. All rates were extrapolated to zero space time. Solid lines show regressed fits of eqs 1 and 2 to the data.

$[GaH]^{2+}$ cations is thermodynamically favored at NNN cation-exchange sites associated with pairs of framework Al atoms ≤5 Å apart.[41] Increasing the Ga/Al ratio results in the formation of $[GaH_2]^+$-H^+ cation pairs at NNN and NNNN cation-exchange sites associated with framework Al−Al interatomic distances >5 Å apart.[41] Our recent theoretical calculations have shown that $[GaH]^{2+}$ cations are more active for C_3H_8 dehydrogenation than $[GaH_2]^+$-H^+ cation pairs.[36] We also note in Figure 3a that the rate of dehydrogenation (per Al_{tot}) over the Ga/Al = 0.5 sample, which contains neutral GaO_x oligomeric species, in addition to cation-exchanged Ga^{3+} species, is identical to the corresponding rate (per Al_{tot}) over samples with lower Ga content. This suggests that neutral GaO_x species are much less active for C_3H_8 conversion in comparison to cation-exchanged Ga^{3+} species.

Based on the foregoing discussion, we normalize the rate of C_3H_8 dehydrogenation by the density of $[GaH]^{2+}$ cations per Al_{tot} for each Ga/Al ratio, measured via NH_3-TPD (see SI S.6 for the method by which the density of $[GaH]^{2+}$ cations was estimated).[41] Figure 3c shows that the rate of C_3H_8 dehydrogenation normalized this way is nearly independent of the Ga/Al ratio. It should be noted that the rate of C_3H_8 dehydrogenation per $[GaH]^{2+}$ for the Ga/Al = 0.05 sample is about 20% higher than that for the remaining samples, which may reflect small differences between the actual fraction of $[GaH]^{2+}$ cations present in the Ga/Al = 0.05 sample and our estimate. We therefore conclude that the rate of C_3H_8 dehydrogenation is approximately independent of the Ga/Al ratio. This finding supports the prediction that $[GaH]^{2+}$ cations are the most active species for C_3H_8 dehydrogenation and that $[GaH_2]^+$-H^+ cation pairs, which constitute an increasing fraction of the Ga content in Ga/H-MFI samples with Ga/Al > 0.1, do not contribute appreciably to the measured rate.[36,41]

Figure 4a−c show C_3H_8 cracking rates over H-MFI and Ga/H-MFI, also measured at 0.9 kPa C_3H_8/He and 733 K. Here again, measured cracking rates over Ga/H-MFI were extrapolated to zero space time. The rate of C_3H_8 cracking normalized per Al_{tot} atom (Figure 4a) shows a trend similar to that of the rate of C_3H_8 dehydrogenation, increasing with Ga content up to a Ga/Al ratio of 0.1 and then reaching a plateau for higher Ga/Al ratios. At similar conditions, the maximum rate of C_3H_8 cracking over Ga/H-MFI (per Al_{tot} atom) is about 20 times higher than that over H-MFI.

It is notable that an enhancement in the rate of alkane cracking over Co-, Zn-, and Ga-exchanged zeolites, relative to the corresponding H-forms of these zeolites, has been reported previously.[15,37,65−67] Alkane cracking over these metal-exchanged zeolites has been attributed to H_2-assisted alkane hydrogenolysis catalyzed by Ga sites[15,66,67] or to protolytic cracking of C−C bonds by residual Brønsted acid O−H groups,[33,37] the acid strength of which may be enhanced by proximity to exchanged metal cations.[68,69] Therefore, both of these possibilities need to be considered as possible causes for the higher rate of C_3H_8 cracking over Ga/H-MFI.

H_2-assisted hydrogenolysis of C_3H_8 would be expected to result in higher cracking rates with increasing H_2 concentration at higher space times (or C_3H_8 conversion) or upon co-feeding H_2. On the contrary, we find that the rate of C_3H_8 cracking decreases with an increase in C_3H_8 conversion and is inhibited by co-feeding H_2 (see Figure S.4 and Section 3.4). These results suggest that hydrogenolysis does not contribute to C_3H_8 cracking over Ga/H-MFI. An alternative explanation is that the higher rate of C_3H_8 cracking over Ga/H-MFI compared to H-MFI could be attributable to an increase in the acid strength of Brønsted acid O−H groups that are proximate to metal cations (here, $[GaH_2]^+$ cations).[68,69] This phenomenon should lead to an increase in the rate of C_3H_8 cracking with an increase in the concentration of $[GaH_2]^+$-H^+ cation pairs as the Ga/Al ratio increases. However, cracking rates normalized per Al_{tot} atom do not increase with Ga content beyond a Ga/Al ratio of 0.1 (Figure 4a), while cracking rates normalized per Ga atom (Figure 4b) decrease monotonically with increasing Ga content. It is also notable that when normalized by the estimated density of $[GaH]^{2+}$ cations per Al_{tot} (see SI S.6 for the method by which the density of $[GaH]^{2+}$ cations was estimated), the rate of C_3H_8 cracking is independent of the Ga/Al ratio, as can be seen in Figure 4c. Taken together, these data suggest that $[GaH]^{2+}$ cations rather than H_2-assisted hydrogenolysis by Ga sites or protolytic cracking by residual Brønsted acid O−H groups proximate to $[GaH_2]^+$ cations, are responsible for the observed

DOI: 10.1021/jacs.8b11443
J. Am. Chem. Soc. 2019, 141, 1614−1627

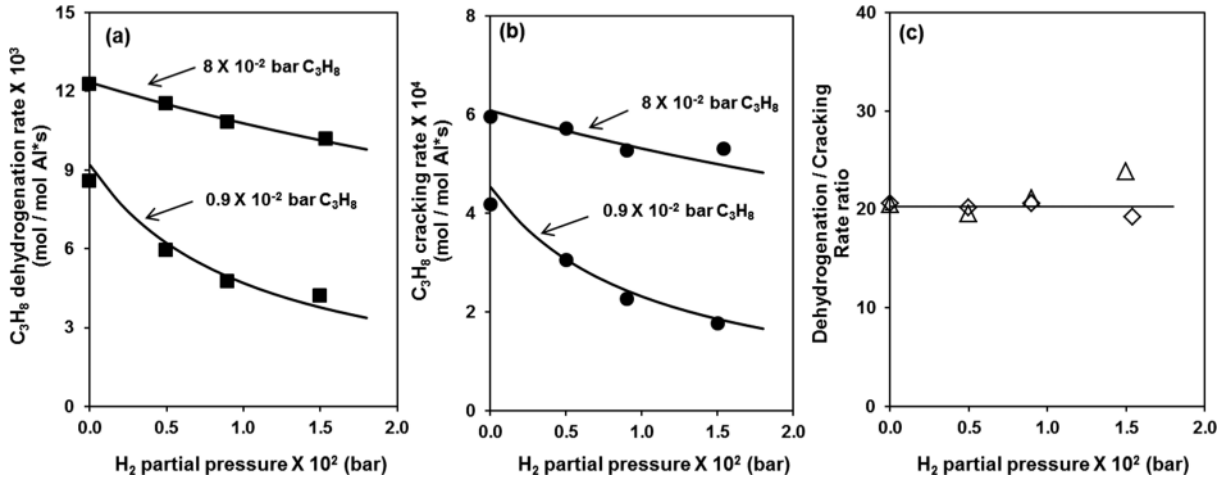

Figure 6. Effects of H_2 partial pressure on the rates of (a) C_3H_8 dehydrogenation and (b) C_3H_8 cracking and (c) the ratio of the rates of dehydrogenation to cracking (D/C) measured at 733 K. All rates were extrapolated to zero space time. In (c), open triangles indicate the D/C ratios measured at 0.9×10^{-2} bar C_3H_8 and open diamonds indicate the D/C rate ratios measured at 8×10^{-2} bar C_3H_8. Solid lines in (a)−(c) show regressed fits of eqs 1 and 2 to the data.

Table 1. Values of Parameters Obtained by Nonlinear Least-Squares Regression of Eqs 1 and 2 to the Rates of C_3H_8 Dehydrogenation and Cracking Measured at 733 K, Shown in Figures 5 and 6[a]

	α (k_{app}) (mol/mol Al_{tot}·s·bar)	β (K_{adsC3}) (bar^{-1})	γ ($K_{ads\ H2}$) (bar^{-1})	α/β (k_{int}) (mol/mol Al_{tot}·s)
dehydrogenation	3.6	2.8×10^2	3.3×10^2	1.3×10^{-2}
cracking	1.8×10^{-1}	2.8×10^2	3.3×10^2	6.4×10^{-4}

[a]The parameters β and γ were common to both dehydrogenation and cracking in eqs 1 and 2, respectively.

enhancements in cracking rates over Ga/H-MFI. Further evidence in support of this conclusion is given below.

3.4. Effects of C_3H_8 and H_2 Partial Pressures on the Rates of C_3H_8 Dehydrogenation and Cracking over Ga/H-MFI. The rates of C_3H_8 dehydrogenation and cracking (per Al_{tot} atom and extrapolated to zero space time) are shown in Figure 5a and b, respectively, as functions of C_3H_8 partial pressure and temperature. At all three temperatures (718, 733, 753 K), the rates of C_3H_8 dehydrogenation and cracking increase monotonically with C_3H_8 partial pressure at low partial pressures but become independent with respect to C_3H_8 partial pressure at higher pressures. Figure 5c shows the dependence of the ratio of the rate of dehydrogenation to cracking (D/C), as a function of the C_3H_8 partial pressure. For a given temperature, no discernible trend is evident in the D/C ratio as a function of C_3H_8 partial pressure, suggesting that the D/C ratio is approximately independent of the surface coverage of adsorbed C_3H_8. This observed trend suggests that both dehydrogenation and cracking proceed over identical active sites in Ga/H-MFI and via a common C_3H_8-derived surface intermediate. However, the D/C ratio does exhibit a weak dependence on temperature, increasing from approximately 19.1 at 753 K to approximately 24.6 at 718 K. An increase in the value of this ratio with a decrease in temperature is consistent with the activation energy for cracking being higher than that for dehydrogenation.

As shown in Figure S.4, H_2 inhibits the rate of C_3H_8 dehydrogenation and cracking over Ga/H-MFI. The dependence of these rates on H_2 partial pressure at 733 K is shown in Figure 6a−c. While the rates of C_3H_8 dehydrogenation and cracking decrease with an increase in H_2 partial pressure, inhibition of these rates is more severe at lower partial pressures of C_3H_8 and relatively weaker at high partial pressures of C_3H_8. Apparent reaction orders of H_2 for dehydrogenation and cracking at each C_3H_8 partial pressure measured at 733 K are provided in Table S1 of the Supporting Information. These effects of H_2 partial pressure are consistent with H_2 competing with C_3H_8 for adsorption on the active sites that catalyze both reactions. As shown in Figure 6c, the D/C ratio is independent of H_2 and C_3H_8 partial pressures, suggesting that H_2 inhibits both dehydrogenation and cracking in a similar fashion and further supports the idea that dehydrogenation and cracking occur on the same active sites.

The observed effects of C_3H_8 and H_2 partial pressures on the rates of C_3H_8 dehydrogenation and cracking are consistent with rate laws of the form given by eqs 1 and 2, respectively. Since the D/C ratio is nearly independent of the C_3H_8 and H_2 partial pressures, the denominator terms in eqs 1 and 2 are taken to be the same.

$$\frac{\text{Dehydrogenation rate}}{Al_{tot}} = \frac{\alpha_d[C_3H_8]}{1 + \beta[C_3H_8] + \gamma[H_2]} \quad (1)$$

$$\frac{\text{Cracking rate}}{Al_{tot}} = \frac{\alpha_c[C_3H_8]}{1 + \beta[C_3H_8] + \gamma[H_2]} \quad (2)$$

Here, α_d (dehydrogenation), α_c (cracking), β, and γ are parameters related to the kinetics and thermodynamics of the elementary steps involved in C_3H_8 dehydrogenation and cracking.

Nonlinear regression of the data shown in Figures 5a−c and 6a−c to eqs 1 and 2, respectively, results in a satisfactory fit, represented by the solid lines in these figures. Values of α_d, α_c, β, and γ at 733 K are presented in Table 1. At very low partial pressures of C_3H_8 and in the absence of co-fed H_2, eqs 1 and 2 and the data in Figures 5 and 6 indicate that the rates of dehydrogenation and cracking exhibit a first-order dependence

DOI: 10.1021/jacs.8b11443
J. Am. Chem. Soc. 2019, 141, 1614−1627

Scheme 1. Alkyl Mechanism for Activation and Dehydrogenation of C_3H_8 over $[GaH]^{2+}$ Sites to C_3H_6 and H_2[a]

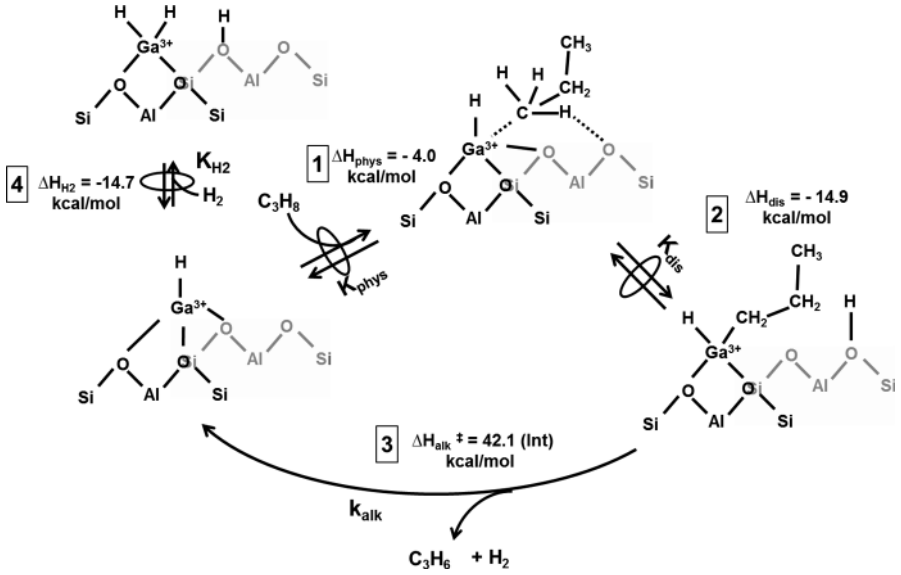

[a]Enthalpies (adsorption, reaction, and activation) for each step are shown here with respect to the enthalpy of the initial structure in the step. For each structure, framework atoms that are faded reflect cation-exchange sites that are behind the image plane for nonfaded cation-exchange sites. Cations coordinated to the faded cation-exchange sites are also behind the image plane but have not been faded for visual purposes.

Scheme 2. Carbenium Mechanism for the Activation and Conversion of C_3H_8 to C_3H_6 and H_2 over $[GaH]^{2+}$ Sites[a]

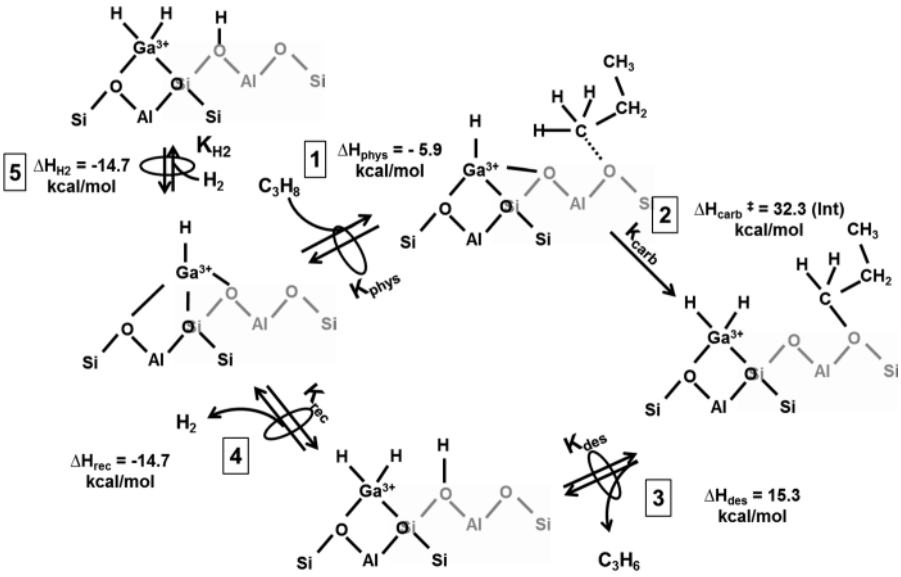

[a]Enthalpies (adsorption, reaction, and activation) for each step are shown here with respect to the enthalpy of the initial structure in the step. For each structure, framework atoms that are faded reflect cation-exchange sites that are behind the image plane for nonfaded cation-exchange sites. Cations coordinated to the faded cation-exchange sites are also behind the image plane but have not been faded for visual purposes.

on C_3H_8 partial pressure. The parameters α_d and α_c therefore reflect apparent first-order rate coefficients (k_{app}) for dehydrogenation and cracking with units of mol/mol Al_{tot}·s·bar. At very high partial pressures of C_3H_8 and in the absence of H_2, the rates of dehydrogenation and cracking are independent of C_3H_8 partial pressure, as seen from the data in Figure 5. In this case, the ratios α_d/β and α_c/β correspond to the zero-order rate coefficients (k_{int}) with units of mol/mol Al_{tot}·s. Therefore, for consistency the parameters β and γ must have units of bar^{-1} and hence correspond to the adsorption coefficients (K_{ads}) for C_3H_8 and H_2, respectively. Further interpretation of the parameters α, β, and γ is discussed below in the context of our examination of possible mechanisms for C_3H_8 dehydrogenation and cracking over Ga/H-MFI.

3.5. Mechanisms for C_3H_8 Dehydrogenation and Cracking over $[GaH]^{2+}$ Sites. Based on the insight gained in Sections 3.3 and 3.4 regarding the role of $[GaH]^{2+}$ cations in catalyzing C_3H_8 dehydrogenation, we can propose two distinct mechanisms by which C_3H_8 undergoes dehydrogenation over $[GaH]^{2+}$ sites: (a) an alkyl mechanism and (b) a carbenium mechanism.[36] In addition, we propose an alkyl mechanism to describe the role of $[GaH]^{2+}$ cations in the cracking of C_3H_8. The elementary steps for the alkyl and carbenium mechanisms for C_3H_8 dehydrogenation and the alkyl mechanism for C_3H_8

DOI: 10.1021/jacs.8b11443
J. Am. Chem. Soc. 2019, 141, 1614−1627

Scheme 3. Cracking of C_3H_8 over $[GaH]^{2+}$ Sites by the Alkyl Mechanism[a]

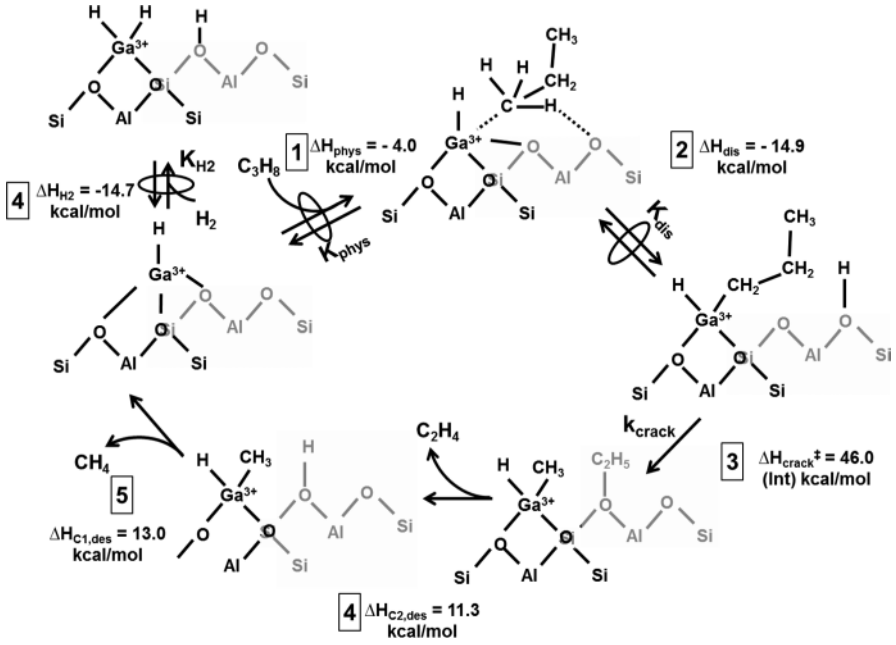

[a]Enthalpies (adsorption, reaction, and activation) for each step are shown here with respect to the enthalpy of the initial structure in the step. For each structure, framework atoms that are faded reflect cation-exchange sites that are behind the image plane for nonfaded cation-exchange sites. Cations coordinated to the faded cation-exchange sites are also behind the image plane but have not been faded for visual purposes.

cracking over $[GaH]^{2+}$ sites are described in Schemes 1, 2, and 3, respectively. Detailed Gibbs free energy and enthalpy reaction coordinate diagrams are also provided for each of the reaction mechanisms in Figures S.6–S.9. The elementary steps presented in Schemes 1–3 can be used to derive rate equations that describe the kinetic behavior predicted by each of the mechanisms, presented here as eq 3 for alkyl-mediated dehydrogenation, eq 4 for carbenium-mediated dehydrogenation, and eq 5 for alkyl-mediated cracking. The assumptions and methods used to derive these equations are described in detail in Section S.4.

$$\frac{\text{Dehydrogenation rate}}{[GaH]^{2+}} = \frac{k_{alk}K_{dis}K_{phys}[C_3H_8]}{1 + (K_{dis}K_{phys})[C_3H_8] + K_{H2}[H_2]} \quad (3)$$

$$\frac{\text{Dehydrogenation rate}}{[GaH]^{2+}} = \frac{k_{carb}K_{phys}[C_3H_8]}{1 + K_{H2}[H_2]} \quad (4)$$

$$\frac{\text{Cracking rate}}{[GaH]^{2+}} = \frac{k_{crack}K_{dis}K_{phys}[C_3H_8]}{1 + (K_{dis}K_{phys})[C_3H_8] + K_{H2}[H_2]} \quad (5)$$

In eqs 3 and 4, k_{alk} and k_{carb} are the rate coefficients for the rate-determining, β-hydride elimination step in the alkyl dehydrogenation sequence (step 3 in Scheme 1) and the rate-determining carbenium C–H activation step in the carbenium dehydrogenation sequence (step 2 in Scheme 2), respectively. In eq 5 k_{crack} is the rate coefficient for the rate-determining C–C bond attack step in the alkyl cracking mechanism (step 3 in Scheme 3). K_{dis} is the equilibrium constant for heterolytic dissociation of C_3H_8 to form $[C_3H_7\text{-}GaH]^+\text{-}H^+$ cation pairs, and K_{phys} is the adsorption constant for C_3H_8 physisorption at $[GaH]^{2+}$ sites. K_{H2} is the equilibrium constant for dissociative adsorption of H_2 at $[GaH]^{2+}$ sites to form $[GaH_2]^+\text{-}H^+$ cation pairs.

As seen in Schemes 1–3, alkyl-mediated pathways for dehydrogenation and cracking over $[GaH]^{2+}$ require dissociative adsorption of C_3H_8 over $[GaH]^{2+}$ to produce $[C_3H_7\text{-}GaH]^+\text{-}H^+$ cation pairs, prior to the rate-determining step. On the other hand, the carbenium-mediated dehydrogenation pathway proceeds via rate-determining C–H activation of C_3H_8 species, physisorbed at $[GaH]^{2+}$. In all three cases, inhibition of rates is predicted to occur via dissociative adsorption of H_2 at $[GaH]^{2+}$ to form $[GaH_2]^+\text{-}H^+$ cation pairs. These observations, together with an inspection of rate equations (3–5) show that only the alkyl-mediated mechanisms predict a first-order dependence of dehydrogenation and cracking rates on C_3H_8 at low C_3H_8 partial pressures and an inhibition of these rates by C_3H_8 at high C_3H_8 partial pressures via the saturation of $[GaH]^{2+}$ sites by strongly bound $[C_3H_7\text{-}GaH]^+$ species. In the carbenium mechanism, the relatively weak binding of C_3H_8 to $[GaH]^{2+}$ sites, prior to the rate-determining C–H activation step, would lead to a first-order dependence of the rate of dehydrogenation on the C_3H_8 partial pressure, in the absence of H_2, as predicted by eq 4.

As seen in Figures 5 and 6, the dependence of the experimentally measured dehydrogenation and cracking rates on C_3H_8 partial pressure is only consistent with the kinetics predicted by the alkyl-mediated mechanisms. Similarly, the D/C rate ratio in Figure 5c and Figure 6c is independent of C_3H_8 and H_2 partial pressures. These observations are also consistent with the conclusion that C_3H_8 dehydrogenation and cracking are catalyzed via a common, strongly bound C_3H_8-derived surface intermediate. The alkyl mechanisms for dehydrogenation and cracking also proceed via a common C_3H_8-derived reactive intermediate, i.e., $[C_3H_7\text{-}GaH]^+\text{-}H^+$ cation pairs.

A further assessment of the relevant mechanisms involved in C_3H_8 dehydrogenation and cracking over Ga/H-MFI can be

DOI: 10.1021/jacs.8b11443
J. Am. Chem. Soc. 2019, 141, 1614–1627

Table 2. Apparent and Intrinsic Activation Enthalpies for C_3H_8 Dehydrogenation and Cracking, and Enthalpies of Dissociative Adsorption for C_3H_8 and H_2, over Ga/H-MFI (Ga/Al = 0.2), extracted from Figures S11−S13 in the SI. Also shown are Theoretically Predicted Activation Enthalpies for C_3H_8 Dehydrogenation and Cracking over $[GaH]^{2+}$ Cations via Alkyl and Carbenium Mechanisms and Predicted Enthalpies of the Dissociative Adsorption of C_3H_8 and H_2 over $[GaH]^{2+}$ Cations[a]

enthalpy (kcal/mol)	dehydrog. experiment[b]	alkyl dehydrog. mechanism[c]	carbenium dehydrog. mechanism[c]	cracking experiment[b]	alkyl cracking mechanism[c]
$\Delta H^{\ddagger}_{app}$	19.0 ± 6.0	23.2	26.4	26.5 ± 0.3	27.1
$\Delta H^{\ddagger}_{int}$	34.6 ± 1.0	42.1	32.3	42.0 ± 4.7	46.0
ΔH_{ads} (C_3H_8)	−15.6 ± 5.0	−18.9	−5.9	−15.6 ± 5.0	−18.9
ΔH_{ads} (H_2)	−7.4 ± 3.3	−14.6	−14.6	−7.4 ± 3.3	−14.6

[a]Reported uncertainties reflect 95% confidence intervals. [b]Obtained from fits of first- and zero-order rate coefficients (k_{app} and k_{int}), measured at 718 K, 733 K and 753 K over the Ga/Al = 0.2 sample, to eqs S24, S25, and S26.[41] [c]Computed using QM/MM methods. See theoretical methods section for more details.

obtained by comparing experimentally derived activation and adsorption enthalpies to their values predicted theoretically. Experimental activation and adsorption enthalpies were obtained by measuring the rates of C_3H_8 dehydrogenation and cracking at different temperatures (718−753 K) over the Ga/Al = 0.2 sample and then determining values of the apparent and intrinsic activation enthalpies for both reactions. The methods used for extracting values of these parameters from kinetic data are provided in Section S.5, and plots showing the temperature dependence of rate coefficients and adsorption coefficients are provided in Figures S.10−S.12.

Experimental values of the activation and adsorption enthalpies for C_3H_8 dehydrogenation and cracking over Ga/H-MFI (Ga/Al = 0.2) are given in Table 2. Also shown in this table are the apparent and intrinsic activation and adsorption enthalpies predicted from QM/MM calculations for the alkyl and carbenium mechanisms for C_3H_8 dehydrogenation and for the alkyl mechanism for C_3H_8 cracking, in all three cases over $[GaH]^{2+}$ sites. For C_3H_8 dehydrogenation, the experimentally measured apparent activation enthalpy is 19.0 ± 6.0 kcal/mol and the intrinsic activation enthalpy is 34.6 ± 1.0 kcal/mol, whereas the adsorption enthalpy for C_3H_8 extracted from experimental data is −15.6 ± 5.0 kcal/mol. These estimates of the C_3H_8 adsorption enthalpy and the apparent and intrinsic enthalpies are consistent with theoretical predictions for the formation of $[C_3H_7\text{-}GaH]^+\text{-}H^+$ cation pairs upon dissociative C_3H_8 adsorption at $[GaH]^{2+}$ sites (−18.9 kcal/mol) and β-hydride elimination of C_3H_6 and H_2 (predicted ΔH_{app} = 23.2 kcal/mol and predicted ΔH_{int} = 42.1 kcal/mol). As noted earlier, the carbenium mechanism involves the activation of an adsorbed C_3H_8 precursor that is weakly bound to the active site, leading to smaller differences between the apparent and intrinsic activation enthalpies than those measured experimentally and to a rate expression for C_3H_8 dehydrogenation that is inconsistent with that observed experimentally (compare eq 1 with eqs 3 and 4).

The DFT-predicted value for the dissociative adsorption of C_3H_8 on $[GaH]^{2+}$ is more exothermic than that for dissociative adsorption of H_2, a finding that is consistent with the experimentally measured adsorption enthalpies reported in Table 2. However, the value for the predicted adsorption enthalpy of H_2 at $[GaH]^{2+}$ sites is lower than that deduced from the analysis of the reaction kinetics. A part of this discrepancy may be due to the sensitivity of the predicted value to the interatomic distance between framework Al atoms involved in proximate cation-exchange sites that host $[GaH]^{2+}$ cations.[35,36] For the NNN Al atom configurations considered, the predicted enthalpy for dissociative adsorption of H_2 over $[GaH]^{2+}$ cations to form $[GaH_2]^+\text{-}H^+$ cation pairs varies between −5.5 and −15.9 kcal/mol. This range encompasses the experimental H_2 adsorption enthalpy value of −7.4 ± 3.3 kcal/mol shown in Table 2.

Table 2 also shows apparent and intrinsic activation enthalpies for C_3H_8 cracking via the alkyl mechanism over $[GaH]^{2+}$ predicted from theoretical calculations. The experimentally measured apparent activation enthalpy (26.5 ± 0.3 kcal/mol) is in excellent agreement with the theoretically predicted estimate (27.1 kcal/mol). The experimentally measured intrinsic activation enthalpy, 42 ± 4.7 kcal/mol, is also in good agreement with the theoretical estimate (44.9 kcal/mol).

The data presented in Table 2 further support the hypothesis that both dehydrogenation and cracking of C_3H_8 over Ga/H-MFI are catalyzed by $[GaH]^{2+}$ sites via a common alkyl-Ga, $[C_3H_7\text{-}GaH]^+$ surface intermediate. Inhibition of both rates occurs by dissociative adsorption of H_2 at $[GaH]^{2+}$ to form $[GaH_2]^+\text{-}H^+$ cation pairs. Consistent with this interpretation, the D/C ratio, shown in Figure 5c and Figure 6c, is independent of C_3H_8 and H_2 surface coverage, but weakly dependent on temperature. Therefore, the selectivity to C_3H_8 dehydrogenation versus cracking over Ga/H-MFI is not governed by the concentrations of C_3H_8, H_2, or residual Brønsted acid O−H groups in Ga/H-MFI, but rather by the difference between the free energy activation barriers for dehydrogenation and cracking over $[GaH]^{2+}$. A higher activation enthalpy for cracking than for dehydrogenation would lead to a decrease in the D/C ratio with an increase in temperature, as observed experimentally in Figure 5c. Indeed, Table 2 indicates that the difference in the measured activation enthalpies (apparent or intrinsic) between cracking and dehydrogenation over Ga/H-MFI, $\Delta\Delta H_{C/D}^{\ddagger}$(exp), is 7.4 ± 4.8 kcal/mol. Consistent with this finding, our theoretical calculations predict a higher activation enthalpy for alkyl-mediated cracking than for alkyl-mediated dehydrogenation ($\Delta\Delta H_{C/D}^{\ddagger}$(calc) = 3.9 kcal/mol).

We turn next to a comparison of our results with those recently reported by Schreiber et al.[37] Ga/H-MFI samples (Si/Al = 50) in their work were prepared using conventional incipient wetness impregnation followed by H_2 reduction. Both C_3H_8 dehydrogenation and cracking rates were shown to increase with Ga content up to a Ga/Al ratio of 0.5, with further increases in Ga content leading to lower rates of dehydrogenation and cracking. Similar to our findings, the rate of C_3H_8 dehydrogenation was shown to exhibit a Langmuir−Hinshelwood dependence on C_3H_8 partial pressure, but the

DOI: 10.1021/jacs.8b11443
J. Am. Chem. Soc. 2019, 141, 1614−1627

dependence of the rate of dehydrogenation on H_2 partial pressure was not investigated.

Schreiber et al. have proposed that Ga^+-H^+ cation pairs are responsible for the dehydrogenation of C_3H_8. This conclusion is based on the observation of a peak at 10 370.2 eV in the XANES spectrum of their sample of H_2-reduced Ga/H-MFI, attributed to Ga^+ cations and to the observation that the rate of dehydrogenation increases with Ga content up to a Ga/Al ratio of 0.5.[37] Periodic DFT calculations were then employed to show how Ga^+-H^+ cation pairs residing at proximate cation-exchange sites associated with NNN pairs of framework Al atoms could catalyze C_3H_8 dehydrogenation. In this scheme, the Ga^+-H^+ cation pair is first converted into a $[GaH]^{2+}$ cation via oxidative addition, and the latter species is assumed to catalyze the alkyl C−H activation of C_3H_8 to form a $[C_3H_7$-$GaH]^+$-H^+ cation pair. This step is then followed by a monomolecular elimination of H_2 from the $[C_3H_7$-$GaH]^+$-H^+ cation pair and subsequent release of C_3H_6 to regenerate Ga^+-H^+ cation pair sites. Both alkyl C−H activation and H_2 elimination steps were reported to be kinetically relevant.

We have examined several aspects of the mechanism proposed by Schieber et al.[37] The first is the ability of $[GaH]^{2+}$ cations to undergo reductive elimination to form Ga^+-H^+ cation pairs. We find that the Gibbs free energy for this reaction is −10.4 kcal/mol and that the free energy barrier for the reductive elimination of H^+ from $[GaH]^{2+}$ to form Ga^+-H^+ cation pairs is 25.2 kcal/mol. This indicates that the formation of Ga^+-H^+ cation pairs from $[GaH]^{2+}$ cations is both thermodynamically and kinetically feasible (see Figure S.8). However, the free energy (77.8 kcal/mol) and enthalpy (26.3 kcal/mol) activation barriers for the C−H activation step via the mechanism reported by Scheiber et al. on the given $[GaH]^{2+}$ site are considerably higher than the corresponding values reported in Scheme 1 and in Figure S7, 40.1 and 2.0 kcal/mol, respectively. We believe that the difference in the energetics reported here and by Scheiber et al.[37] is a consequence of how $[GaH]^{2+}$ cations are coordinated with the zeolite framework. In the latter study, $[GaH]^{2+}$ cations are bound to two framework O atoms, whereas in our work, $[GaH]^{2+}$ cations are bound to three framework O atoms (and one H ligand), thus forming the preferred tetrahedral coordination around the Ga^{3+} center.[70] The three framework O atoms in the first coordination sphere of these species withdraw more electron density from the Ga^{3+} center, resulting in $[GaH]^{2+}$ cations that are more Lewis acidic and therefore more reactive toward alkane C−H activation than $[GaH]^{2+}$ cations that are bound to only two framework O atoms.

We have also investigated the free energy landscape for the dehydrogenation pathway over Ga^+-H^+ cation pairs proposed by Schreiber et al. Our calculations indicate that the rate-determining step for this sequence is the concerted elimination of C_3H_6 and H_2 from $[C_3H_7$-$GaH]^+$-H^+ cation pairs to re-form Ga^+-H^+ cation pairs (see Figure S8). The Gibbs free energy barrier for this rate-determining transition state is about 20 kcal/mol higher than that for the rate-determining step in the alkyl sequence over $[GaH]^{2+}$ shown in Scheme 1 (see Figure S7), thereby rendering the former pathway less favorable. Thus, while our theoretical calculations predict that the formation of Ga^+-H^+ cation pairs from $[GaH]^{2+}$ cations is thermodynamically and kinetically feasible, these calculations also predict that the dehydrogenation of C_3H_8 via processes involving Ga^+-H^+ cation pairs would be much less favorable than those involving $[GaH]^{2+}$ cations. We also show that while Ga^+-H^+ cation pairs can activate C_3H_8 to produce $[C_3H_7$-$GaH]^+$-H^+ cation pairs, the barrier to form $[GaH]^{2+}$ cations from $[C_3H_7$-$GaH]^+$-H^+ cation pairs is much lower than that to regenerate Ga^+-H^+ cation pairs (see Figure S15). Therefore, our findings strongly suggest that $[GaH]^{2+}$ cations are the primary active sites responsible for dehydrogenation.

4. CONCLUSIONS

The kinetics of C_3H_8 dehydrogenation and cracking were investigated over Ga/H-MFI, prepared with Ga/Al ratios between 0.05 and 0.3, for which all of the Ga is presented as isolated cationic species. C_3H_8 conversion occurs over H-MFI via monomolecular dehydrogenation and cracking catalyzed by Brønsted O−H acid groups. C_3H_8 conversion over preoxidized Ga/H-MFI undergoes an induction period before reaching a steady-state activity. The induction period is significantly attenuated by prereducing the catalysts in H_2. Notably, the distribution of products formed via C_3H_8 dehydrogenation and cracking is virtually unchanged during the induction period, and the steady-state activities of Ga/H-MFI are independent of the initial state of cationic Ga^{3+} species (oxidized or reduced). Reaction rates (expressed per Al_{tot} atom) for C_3H_8 dehydrogenation and cracking over Ga/H-MFI (Ga/Al = 0.2) are ∼500 and ∼20 times, respectively, higher than the corresponding rates over H-MFI at identical conditions. Rates of both reactions when normalized with respect to the concentration of $[GaH]^{2+}$ cations are found to be independent of the Ga/Al ratio, suggesting that $[GaH]^{2+}$ cations are the catalytically active centers for both reactions. C_3H_8 dehydrogenation and cracking rates over Ga/H-MFI are first-order in C_3H_8 at low C_3H_8 partial pressures and are inhibited by C_3H_8 at higher C_3H_8 partial pressures. Both reactions are inhibited by the presence of H_2. Ratios of the rates of dehydrogenation to cracking (D/C) are, however, independent of the partial pressures of C_3H_8 and H_2 and only dependent upon temperature, again suggesting that both reactions involve the same active center. The observed dependences of reaction rates on the partial pressures of C_3H_8 and H_2 as well as both the apparent and intrinsic activation enthalpies are consistent with theoretical predictions based on a proposed alkyl-mediated mechanism for the two reactions. The alkyl-mediated mechanism for C_3H_8 dehydrogenation and cracking begins with the reversible, dissociative adsorption of C_3H_8 at $[GaH]^{2+}$ to form $[C_3H_7$-$GaH]^+$-H^+ cation pairs. Dehydrogenation then proceeds via rate-determining β-hydride elimination from the C_3H_7 fragment to form C_3H_6 and H_2 in a concerted step involving a cyclic transition state. On the other hand, cracking proceeds via rate-determining C−C bond attack of the C_3H_7 fragment by the proximal Brønsted acid O−H group, resulting in the formation of $[CH_3$-$GaH]^+$ cations proximal to ethoxide species. C_2H_4 and CH_4 are then formed in subsequent steps that are not kinetically relevant. Inhibition of both dehydrogenation and cracking by H_2 occurs via dissociative adsorption of H_2 at $[GaH]^{2+}$ cations to produce $[GaH_2]^+$-H^+ cation pairs, which are much less active for C_3H_8 dehydrogenation and cracking.

■ ASSOCIATED CONTENT

Supporting Information

The Supporting Information is available free of charge on the ACS Publications website at DOI: 10.1021/jacs.8b11443.

DOI: 10.1021/jacs.8b11443
J. Am. Chem. Soc. 2019, 141, 1614−1627

Details regarding characterization, catalytic rate measurements, and theoretical calculations (PDF)

AUTHOR INFORMATION

Corresponding Author

*alexbell@berkeley.edu

ORCID

Martin Head-Gordon: 0000-0002-4309-6669

Alexis T. Bell: 0000-0002-5738-4645

Author Contributions

⊥N. M. Phadke and E. Mansoor contributed equally to this work.

Notes

The authors declare no competing financial interest.

ACKNOWLEDGMENTS

This work was supported by Chevron Energy Technology Company. Computational resources were provided by the Molecular Graphics and Computation Facility (supported by NIH S10OD023532). We would like to thank Christopher Ho for helpful technical discussions. E.M. gratefully acknowledges support from the Abu Dhabi National Oil Company in the form of a fellowship. M.B. acknowledges support provided to him as a visiting scholar by Prof. Liubov Kiwi-Minsker of the Ecole Polytechnique Federale de Lausanne, Lausanne, Switzerland.

REFERENCES

(1) Siirola, J. J. The Impact of Shale Gas in the Chemical Industry. *AIChE J.* **2014**, *60*, 810−819.

(2) Al-Douri, A.; Sengupta, D.; El-Halwagi, M. M. Shale Gas Monetization − A Review of Downstream Processing to Chemicals and Fuels. *J. Nat. Gas Sci. Eng.* **2017**, *45*, 436−455.

(3) Sousa-Aguiar, E. F.; Noronha, F. B.; Faro, A. The Main Catalytic Challenges in GTL (Gas-to-Liquids) Processes. *Catal. Sci. Technol.* **2011**, *1*, 698−713.

(4) Sattler, J. J. H. B.; Ruiz-Martinez, J.; Santillan-Jimenez, E.; Weckhuysen, B. M. Catalytic Dehydrogenation of Light Alkanes on Metals and Metal Oxides. *Chem. Rev.* **2014**, *114*, 10613−10653.

(5) Guisnet, M.; Gnep, N. S.; Alario, F. Aromatization of Short Chain Alkanes on Zeolite Catalysts. *Appl. Catal., A* **1992**, *89*, 1−30.

(6) Al-Zahrani, S. M. Catalytic Conversion of LPG to High-Value Aromatics: The Current State of the Art and Future Predictions. *Dev. Chem. Eng. Miner. Process.* **1998**, *6*, 101−120.

(7) Guisnet, M.; Gnep, N. S. Aromatization of Propane over GaHMFI Catalysts. Reaction Scheme, Nature of the Dehydrogenating Species and Mode of Coke Formation. *Catal. Today* **1996**, *31*, 275−292.

(8) Price, G. L.; Kanazirev, V. Ga_2O_3/HZSM-5 Propane Aromatization Catalysts: Formation of Active Centers via Solid-State Reaction. *J. Catal.* **1990**, *126*, 267−278.

(9) Meitzner, G. D.; Iglesia, E.; Baumgartner, J. E.; Huang, E. S. The Chemical State of Gallium in Working Alkane Dehydrocyclodimerization Catalysts. *J. Catal.* **1993**, *140*, 209−225.

(10) Biscardi, J. A.; Iglesia, E. Structure and Function of Metal Cations in Light Alkane Reactions Catalyzed by Modified H-ZSM5. *Catal. Today* **1996**, *31*, 207−231.

(11) Anderson, R. F.; Johnson, J. A.; Mowry, J. R. Cyclar: One Step Processing of LPG to Aromatics and Hydrogen. In *Institute of Chemical Engineering, Spring National Meeting*; Houston, TX; 1985.

(12) Hensen, E. J. M.; Pidko, E. A.; Rane, N.; van Santen, R. A. Modification of Brønsted Acidity of Zeolites by Ga^+, GaO^+ and AlO^+: Comparison for Alkane Activation. In *Studies in Surface Science Catalysis*; Elsevier B.V.: Beijing, 2007; Vol. *170*, pp 1182−1189.

(13) Faro, C.; Oliveira, V. *Stud. Surf. Sci. Catal.* **2008**, *174*, 1155−1158.

(14) De, O.; Rodrigues, V.; Eon, J. G.; Faro, A. C. Correlations between Dispersion, Acidity, Reducibility, and Propane Aromatization Activity of Gallium Species Supported on HZSM5 Zeolites. *J. Phys. Chem. C* **2010**, *114*, 4557−4567.

(15) Rodrigues, V. D. O.; Faro Júnior, A. C. On Catalyst Activation and Reaction Mechanisms in Propane Aromatization on Ga/HZSM5 Catalysts. *Appl. Catal., A* **2012**, *435*−*436*, 68−77.

(16) Taha, Z. A.; Deguns, E. W.; Chattopadhyay, S.; Scott, S. L. Formation of Digallium Sites in the Reaction of Trimethylgallium with Silica. *Organometallics* **2006**, *25*, 1891−1899.

(17) Szeto, K. C.; Gallo, A.; Hernández-Morejudo, S.; Olsbye, U.; De Mallmann, A.; Lefebvre, F.; Gauvin, R. M.; Delevoye, L.; Scott, S. L.; Taoufik, M. Selective Grafting of $Ga(i\text{-}Bu)_3$ on the Silanols of Mesoporous H-ZSM-5 by Surface Organometallic Chemistry. *J. Phys. Chem. C* **2015**, *119*, 26611−26619.

(18) Getsoian, A. B.; Das, U.; Camacho-Bunquin, J.; Zhang, G.; Gallagher, J. R.; Hu, B.; Cheah, S.; Schaidle, J. A.; Ruddy, D. A.; Hensley, J. E.; Krause, T. R.; Curtiss, L. A.; Miller, J. T.; Hock, A. S. Organometallic Model Complexes Elucidate the Active Gallium Species in Alkane Dehydrogenation Catalysts Based on Ligand Effects in Ga K-Edge XANES. *Catal. Sci. Technol.* **2016**, *101*, 12−18.

(19) Cybulskis, V. J.; Pradhan, S. U.; Lovón-Quintana, J. J.; Hock, A. S.; Hu, B.; Zhang, G.; Delgass, W. N.; Ribeiro, F. H.; Miller, J. T. The Nature of the Isolated Gallium Active Center for Propane Dehydrogenation on Ga/SiO_2. *Catal. Lett.* **2017**, *147*, 1252−1262.

(20) Searles, K.; Siddiqi, G. G.; Safonova, O. V.; Coperet, C. Silica-Supported Isolated Gallium Sites as Highly Active, Selective and Stable Propane Dehydrogenation Catalysts. *Chem. Sci.* **2017**, *8*, 2661−2666.

(21) Kim, W. G.; So, J.; Choi, S. W.; Liu, Y.; Dixit, R. S.; Sievers, C.; Sholl, D. S.; Nair, S.; Jones, C. W. Hierarchical Ga-MFI Catalysts for Propane Dehydrogenation. *Chem. Mater.* **2017**, *29*, 7213−7222.

(22) Schreiber, M. W.; Plaisance, C. P.; Baumgärtl, M.; Reuter, K.; Jentys, A.; Bermejo-Deval, R.; Lercher, J. A. Lewis-Brønsted Acid Pairs in Ga/H-ZSM-5 to Catalyze Dehydrogenation of Light Alkanes. *J. Am. Chem. Soc.* **2018**, *140*, 4849−4859.

(23) Bhan, A.; Nicholas Delgass, W. Propane Aromatization over HZSM-5 and Ga/HZSM-5 Catalysts. *Catal. Rev.: Sci. Eng.* **2008**, *50*, 19−151.

(24) Dooley, K. M.; Chang, C.; Price, G. L. Effects of Pretreatments on State of Gallium and Aromatization Activity of Gallium/ZSM-5 Catalysts. *Appl. Catal., A* **1992**, *84*, 17−30.

(25) Dooley, K. M.; Price, G. L.; Kanazirev, V. I.; Hart, V. I. Gallium-Loaded Zeolites for Light Paraffin Aromatization: Evidence for Exchanged Gallium Cation Active Centers. *Catal. Today* **1996**, *31*, 305−315.

(26) Price, G. L.; Kanazirev, V.; Dooley, K. M.; Hart, V. I. On the Mechanism of Propane Dehydrocyclization over Cation-Containing, Proton-Poor MFI Zeolite. *J. Catal.* **1998**, *173*, 17−27.

(27) Pidko, E. A.; Kazansky, V. B.; Hensen, E. J. M.; van Santen, R. A. A Comprehensive Density Functional Theory Study of Ethane Dehydrogenation over Reduced Extra-Framework Gallium Species in ZSM-5 Zeolite. *J. Catal.* **2006**, *240*, 73−84.

(28) Kazansky, V. B.; Subbotina, I. R.; Van Santen, R. A.; Hensen, E. J. M. DRIFTS Study of the Nature and Chemical Reactivity of Gallium Ions in Ga/ZSM-5: II. Oxidation of Reduced Ga Species in ZSM-5 by Nitrous Oxide or Water. *J. Catal.* **2005**, *233*, 351−358.

(29) Rane, N.; Overweg, A. R.; Kazansky, V. B.; van Santen, R. A.; Hensen, E. J. M. Characterization and Reactivity of Ga^+ and GaO^+ Cations in Zeolite ZSM-5. *J. Catal.* **2006**, *239*, 478−485.

(30) Hensen, E. J. M.; Pidko, E. A.; Rane, N.; Van Santen, R. A. Water-Promoted Hydrocarbon Activation Catalyzed by Binuclear Gallium Sites in ZSM-5 Zeolite. *Angew. Chem., Int. Ed.* **2007**, *46*, 7273−7276.

(31) Pidko, E. a.; Hensen, E. J. M.; van Santen, R. A. Self-Organization of Extraframework Cations in Zeolites. *Proc. R. Soc. London, Ser. A* **2012**, *468*, 2070−2086.

DOI: 10.1021/jacs.8b11443
J. Am. Chem. Soc. 2019, 141, 1614−1627

(32) Joshi, Y. V.; Thomson, K. T. The Roles of Gallium Hydride and Brønsted Acidity in Light Alkane Dehydrogenation Mechanisms Using Ga-Exchanged HZSM-5 Catalysts: A DFT Pathway Analysis. *Catal. Today* **2005**, *105*, 106−121.
(33) Rane, N.; Kersbulck, M.; van Santen, R. A.; Hensen, E. J. M. Cracking of N-Heptane over Brønsted Acid Sites and Lewis Acid Ga Sites in ZSM-5 Zeolite. *Microporous Mesoporous Mater.* **2008**, *110*, 279−291.
(34) Faro, A. C.; Rodrigues, V. D. O.; Eon, J. G. In Situ X-Ray Absorption Study of the Genesis and Nature of the Reduced Gallium Species in Ga/HZSM5 Catalysts. *J. Phys. Chem. C* **2011**, *115*, 4749−4756.
(35) Joshi, Y. V.; Thomson, K. T. High Ethane Dehydrogenation Activity of $[GaH]^{2+}$ Al Pair Sites in Ga/H-[Al]ZSM-5: A DFT Thermochemical Analysis of the Catalytic Sites under Reaction Conditions. *J. Catal.* **2007**, *246*, 249−265.
(36) Mansoor, E.; Head-Gordon, M.; Bell, A. T. Computational Modeling of the Nature and Role of Ga Species for Light Alkane Dehydrogenation Catalyzed by Ga/H-MFI. *ACS Catal.* **2018**, *8*, 6146−6162.
(37) Schreiber, M. W.; Plaisance, C. P.; Baumgärtl, M.; Reuter, K.; Jentys, A.; Bermejo-Deval, R.; Lercher, J. A. Lewis-Brønsted Acid Pairs in Ga/H-ZSM-5 to Catalyze Dehydrogenation of Light Alkanes. *J. Am. Chem. Soc.* **2018**, *140*, 4849−4859.
(38) Gonzales, N. O.; Chakraborty, A. K.; Bell, A. T. A Density Functional Theory Study of Hydrogen Recombination and Hydrogen-Deuterium Exchange on Ga/H-ZSM-5. *Top. Catal.* **1999**, *9*, 207−213.
(39) Meriaudeau, P.; Naccache, C. H-ZSM-5 Supported Ga_2O_3 Dehydrocyclisation Catalysts Infrared Spectroscopic Evidence of Gallium Oxide Surface Mobility. *Appl. Catal.* **1991**, *73*, 13−18.
(40) Joly, J. F.; Ajot, H.; Merlen, E.; Raatz, F.; Alario, F. Parameters Affecting the Dispersion of the Gallium Phase of Gallium H-MFI Aromatization Catalysts. *Appl. Catal., A* **1991**, *79*, 249−263.
(41) Phadke, N.; Van Der Mynsbrugge, J.; Mansoor, E.; Getsoian, A.; Head-Gordon, M.; Bell, A. T. Characterization of Isolated Ga^{3+} Cations in Ga/H-MFI Prepared by Vapor-Phase Exchange of H-MFI with $GaCl_3$. *ACS Catal.* **2018**, *8*, 6106−6126.
(42) Vannice, A. M. *Kinetics of Catalytic Reactions*; Springer US: New York, 2005; pp 1−257.
(43) Mallikarjun Sharada, S.; Zimmerman, P. M.; Bell, A. T.; Head-Gordon, M. Insights into the Kinetics of Cracking and Dehydrogenation Reactions of Light Alkanes in H-MFI. *J. Phys. Chem. C* **2013**, *117*, 12600−12611.
(44) Zimmerman, P. M.; Head-Gordon, M.; Bell, A. T. Selection and Validation of Charge and Lennard-Jones Parameters for QM/MM Simulations of Hydrocarbon Interactions with Zeolites. *J. Chem. Theory Comput.* **2011**, *7*, 1695−1703.
(45) Mansoor, E.; Van der Mynsbrugge, J.; Head-Gordon, M.; Bell, A. T. Impact of Long-Range Electrostatic and Dispersive Interactions on Theoretical Predictions of Adsorption and Catalysis in Zeolites. *Catal. Today* **2018**, *312*, 51−65.
(46) Li, Y.-P.; Gomes, J.; Mallikarjun Sharada, S.; Bell, A. T.; Head-Gordon, M. Improved Force-Field Parameters for QM/MM Simulations of the Energies of Adsorption for Molecules in Zeolites and a Free Rotor Correction to the Rigid Rotor Harmonic Oscillator Model for Adsorption Enthalpies. *J. Phys. Chem. C* **2015**, *119*, 1840−1850.
(47) Olson, D. H.; Khosrovani, N.; Peters, A. W.; Toby, B. H. Crystal Structure of Dehydrated CsZSM-5 (5.8Al): Evidence for Nonrandom Aluminum Distribution. *J. Phys. Chem. B* **2000**, *104*, 4844−4848.
(48) Gomes, J.; Zimmerman, P. M.; Head-Gordon, M.; Bell, A. T. Accurate Prediction of Hydrocarbon Interactions with Zeolites Utilizing Improved Exchange-Correlation Functionals and QM/MM Methods: Benchmark Calculations of Adsorption Enthalpies and Application to Ethene Methylation by Methanol. *J. Phys. Chem. C* **2012**, *116*, 15406−15414.
(49) Shao, Y.; Gan, Z.; Epifanovsky, E.; Gilbert, A. T. B.; Wormit, M.; Kussmann, J.; Lange, A. W.; Behn, A.; Deng, J.; Feng, X.; Ghosh, D.; Goldey, M.; Horn, P. R.; Jacobson, L. D.; Kaliman, I.; Khaliullin, R. Z.; Kuś, T.; Landau, A.; Liu, J.; Proynov, E. I.; Rhee, Y. M.; Richard, R. M.; Rohrdanz, M. A.; Steele, R. P.; Sundstrom, E. J.; Woodcock, H. L.; Zimmerman, P. M.; Zuev, D.; Albrecht, B.; Alguire, E.; Austin, B.; Beran, G. J. O.; Bernard, Y. A.; Berquist, E.; Brandhorst, K.; Bravaya, K. B.; Brown, S. T.; Casanova, D.; Chang, C.-M.; Chen, Y.; Chien, S. H.; Closser, K. D.; Crittenden, D. L.; Diedenhofen, M.; DiStasio, R. A.; Do, H.; Dutoi, A. D.; Edgar, R. G.; Fatehi, S.; Fusti-Molnar, L.; Ghysels, A.; Golubeva-Zadorozhnaya, A.; Gomes, J.; Hanson-Heine, M. W. D.; Harbach, P. H. P.; Hauser, A. W.; Hohenstein, E. G.; Holden, Z. C.; Jagau, T.-C.; Ji, H.; Kaduk, B.; Khistyaev, K.; Kim, J.; Kim, J.; King, R. A.; Klunzinger, P.; Kosenkov, D.; Kowalczyk, T.; Krauter, C. M.; Lao, K. U.; Laurent, A. D.; Lawler, K. V.; Levchenko, S. V.; Lin, C. Y.; Liu, F.; Livshits, E.; Lochan, R. C.; Luenser, A.; Manohar, P.; Manzer, S. F.; Mao, S.-P.; Mardirossian, N.; Marenich, A. V.; Maurer, S. A.; Mayhall, N. J.; Neuscamman, E.; Oana, C. M.; Olivares-Amaya, R.; O'Neill, D. P.; Parkhill, J. A.; Perrine, T. M.; Peverati, R.; Prociuk, A.; Rehn, D. R.; Rosta, E.; Russ, N. J.; Sharada, S. M.; Sharma, S.; Small, D. W.; Sodt, A.; Stein, T.; Stück, D.; Su, Y.-C.; Thom, A. J. W.; Tsuchimochi, T.; Vanovschi, V.; Vogt, L.; Vydrov, O.; Wang, T.; Watson, M. A.; Wenzel, J.; White, A.; Williams, C. F.; Yang, J.; Yeganeh, S.; Yost, S. R.; You, Z.-Q.; Zhang, I. Y.; Zhang, X.; Zhao, Y.; Brooks, B. R.; Chan, G. K. L.; Chipman, D. M.; Cramer, C. J.; Goddard, W. A.; Gordon, M. S.; Hehre, W. J.; Klamt, A.; Schaefer, H. F.; Schmidt, M. W.; Sherrill, C. D.; Truhlar, D. G.; Warshel, A.; Xu, X.; Aspuru-Guzik, A.; Baer, R.; Bell, A. T.; Besley, N. A.; Chai, J.-D.; Dreuw, A.; Dunietz, B. D.; Furlani, T. R.; Gwaltney, S. R.; Hsu, C.-P.; Jung, Y.; Kong, J.; Lambrecht, D. S.; Liang, W.; Ochsenfeld, C.; Rassolov, V. A.; Slipchenko, L. V.; Subotnik, J. E.; Van Voorhis, T.; Herbert, J. M.; Krylov, A. I.; Gill, P. M. W.; Head-Gordon, M. Advances in Molecular Quantum Chemistry Contained in the Q-Chem 4 Program Package. *Mol. Phys.* **2015**, *113*, 184−215.
(50) Chai, J.-D.; Head-Gordon, M. Long-Range Corrected Hybrid Density Functionals with Damped Atom−atom Dispersion Corrections. *Phys. Chem. Chem. Phys.* **2008**, *10*, 6615−6620.
(51) Mardirossian, N.; Head-Gordon, M. Thirty Years of Density Functional Theory in Computational Chemistry: An Overview and Extensive Assessment of 200 Density Functionals. *Mol. Phys.* **2017**, *115*, 2315−2372.
(52) Goerigk, L.; Hansen, A.; Bauer, C. A.; Ehrlich, S.; Najibi, A.; Grimme, S. A Look at the Density Functional Theory Zoo with the Advanced GMTKN55 Database for General Main Group Thermochemistry, Kinetics and Noncovalent Interactions. *Phys. Chem. Chem. Phys.* **2017**, *19*, 32184−32215.
(53) Janda, A.; Vlaisavljevich, B.; Lin, L. C.; Mallikarjun Sharada, S.; Smit, B.; Head-Gordon, M.; Bell, A. T. Adsorption Thermodynamics and Intrinsic Activation Parameters for Monomolecular Cracking of N-Alkanes on Brønsted Acid Sites in Zeolites. *J. Phys. Chem. C* **2015**, *119*, 10427−10438.
(54) Kozuch, S. A Refinement of Everyday Thinking: The Energetic Span Model for Kinetic Assessment of Catalytic Cycles. *Wiley Interdiscip. Rev. Comput. Mol. Sci.* **2012**, *2*, 795−815.
(55) Kozuch, S.; Shaik, S. How to Conceptualize Catalytic Cycles? The Energetic Span Model. *Acc. Chem. Res.* **2011**, *44*, 101−110.
(56) Kozuch, S.; Martin, J. M. L. Turning Over " Definitions in Catalytic Cycles. *ACS Catal.* **2012**, *2*, 2787−2794.
(57) Kozuch, S.; Shaik, S. A Combined Kinetic-Quantum Mechanical Model for Assessment of Catalytic Cycles: Application to Cross-Coupling and Heck Reactions. *J. Am. Chem. Soc.* **2006**, *128*, 3355−3365.
(58) Janda, A.; Bell, A. T. Effects of Si/Al Ratio on the Distribution of Framework Al and on the Rates of Alkane Monomolecular Cracking and Dehydrogenation in H-MFI. *J. Am. Chem. Soc.* **2013**, *135*, 19193−19207.
(59) Narbeshuber, T. F.; Vinek, H.; Lercher, J. A. Monomolecular Conversion of Light Alkanes over H-ZSM-5. *J. Catal.* **1995**, *157*, 388−395.

DOI: 10.1021/jacs.8b11443
J. Am. Chem. Soc. 2019, 141, 1614−1627

(60) Gounder, R.; Iglesia, E. Catalytic Consequences of Spatial Constraints and Acid Site Location for Monomolecular Alkane Activation on Zeolites. *J. Am. Chem. Soc.* **2009**, *131*, 1958−1971.
(61) Haag, W. O.; Dessau, R. M.; Lago, R. M. Kinetics and Mechanism of Paraffin Cracking with Zeolite Catalysts. *Stud. Surf. Sci. Catal.* **1991**, *60*, 255−265.
(62) Kotrel, S.; Knözinger, H.; Gates, B. C. The Haag-Dessau Mechanism of Protolytic Cracking of Alkanes. *Microporous Mesoporous Mater.* **2000**, *35*−*36*, 11−20.
(63) Narbeshuber, T. F.; Brait, A.; Seshan, K.; Lercher, J. A. Dehydrogenation of Light Alkanes over Zeolites. *J. Catal.* **1997**, *172*, 127−136.
(64) Xu, B.; Sievers, C.; Hong, S. B.; Prins, R.; van Bokhoven, J. A. Catalytic Activity of Brønsted Acid Sites in Zeolites: Intrinsic Activity, Rate-Limiting Step, and Influence of the Local Structure of the Acid Sites. *J. Catal.* **2006**, *244*, 163−168.
(65) Li, W.; Yu, S. Y.; Meitzner, G. D.; Iglesia, E. Structure and Properties of Cobalt-Exchanged H-ZSM5 Catalysts for Dehydrogenation and Dehydrocyclization of Alkanes. *J. Phys. Chem. B* **2001**, *105*, 1176−1184.
(66) Kolyagin, Y. G.; Ordomsky, V. V.; Khimyak, Y. Z.; Rebrov, A. I.; Fajula, F.; Ivanova, I. I. Initial Stages of Propane Activation over Zn/MFI Catalyst Studied by in Situ NMR and IR Spectroscopic Techniques. *J. Catal.* **2006**, *238*, 122−133.
(67) Gabrienko, A. A.; Arzumanov, S. S.; Freude, D.; Stepanov, A. G. Propane Aromatization on Zn-Modified Zeolite BEA Studied by Solid-State NMR in Situ. *J. Phys. Chem. C* **2010**, *114*, 12681−12688.
(68) Gonzales, N. O.; Chakraborty, A. K.; Bell, A. T. A Density Functional Study of the Effects of Metal Cations on the Bronsted Acidity of H-ZSM-5. *Catal. Lett.* **1998**, *50*, 135−139.
(69) Vayssilov, G. N.; Rösch, N. Influence of Alkali and Alkaline Earth Cations on the Brønsted Acidity of Zeolites. *J. Phys. Chem. B* **2001**, *105*, 4277−4284.
(70) Wilkinson, G.; Gillard, R. D.; McCleverty, J. A. *Comprehensive Coordination Chemistry: The Synthesis, Reactions, Properties & Applications of Coordination Compounds*; Pergamon Press, 1987; pp 1−1601.

DOI: 10.1021/jacs.8b11443
J. Am. Chem. Soc. 2019, 141, 1614−1627